Proceedings of IMECE'2002
2002 ASME International Mechanical Engineering Congress & Exposition
New Orleans, Louisiana, November 17-22, 2002

IMECE2002-33704

EXAMINATION OF THE SLIP BOUNDARY CONDITION BY μ-PIV AND LATTICE BOLTZMANN SIMULATIONS

Derek C. Tretheway, Luoding Zhu, Linda Petzold, and Carl D. Meinhart
Department of Mechanical and Environmental Engineering
University of California Santa Barbara
Santa Barbara, CA 93106
Email: meinhart@engineering.ucsb.edu

ABSTRACT

This work examines the slip boundary condition by Lattice Boltzmann simulations, addresses the validity of the Navier's hypothesis that the slip velocity is proportional to the shear rate and compares the Lattice Boltzmann simulations to the experimental results of Tretheway and Meinhart (Phys. of Fluids, **14**, L9-L12). The numerical simulation models the boundary condition as the probability, *P*, of a particle to bounce-back relative to the probability of specular reflection, 1-*P*. For channel flow, the numerically calculated velocity profiles are consistent with the experimental profiles for both the no-slip and slip cases. No-slip is obtained for a probability of 100% bounce-back, while a probability of 0.03 is required to generate a slip length and slip velocity consistent with the experimental results of Tretheway and Meinhart for a hydrophobic surface. The simulations indicate that for microchannel flow the slip length is nearly constant along the channel walls, while the slip velocity varies with wall position as a results of variations in shear rate. Thus, the resulting velocity profile in a channel flow is more complex than a simple combination of the no-slip solution and slip velocity as is the case for flow between two infinite parallel plates.

NOMENCLATURE

P	probability for particle bounce-back
h	half height of plate separation
t	time
v	velocity
w_j	weighting factor
x	streamwise direction
x	space coordinate
y	spanwise direction
$f(\mathbf{x},\boldsymbol{\xi},t)$	particle distribution function
β	slip length
ρ	density
τ	relaxation time
ξ	particle velocity space
Δt	time step

INTRODUCTION

For nearly a hundred years scientists and engineers have applied the no-slip boundary condition to fluid flow over a solid surface. While the generally-accepted no-slip boundary condition has been validated experimentally for a number of macroscopic flows, it remains an assumption not based on physical principles. In fact, nearly two hundred years ago, Navier [1] proposed a more general boundary condition, which includes the possibility of fluid slip. Navier's proposed boundary condition assumes that the velocity, v_x, at a solid surface is proportional to the shear rate at the surface,

$$v_x = \beta(dv_x/dy) \qquad (1)$$

where β is the slip length or slip coefficient. If β=0 then the generally assumed no-slip boundary condition is obtained. If β is finite, fluid slip occurs at the wall, but its effect depends upon the length scale of the flow. For example, the solution for Stokes flow between two infinite parallel plates with the boundary conditions of no shear stress at the centerline and Navier's hypothesis (1) at the wall, yields

$$v_x = \frac{h^2}{2\mu}\left(-\frac{dp}{dx}\right)\left[\left(1-\left(\frac{y}{h}\right)^2\right)+\frac{2\beta}{h}\right], \qquad (2)$$

where $2h$ is the distance between the two plates, μ is the viscosity, and $(-dp/dx)$ is the pressure drop. The first term in the brackets, $1-(y/h)^2$, is the standard solution for pressure-driven Stokes flow between two infinite parallel plates with no-slip, while the second term, $2\beta/h$, represents an additional velocity associated with the general boundary condition (1). The first term is of order one while the second term depends on the plate separation, h. If β is finite, the importance of the second term increases as h decreases, and for a given β, there is a sufficiently small length scale at which this term not only becomes comparable to the first, but dominates equation (2). Since the no-slip assumption appears to be valid at the macroscale, β must be relatively small for Navier's hypothesis to hold. However, it's not readily apparent that the second term in equation (2) will remain negligible for flows in microdevices where the characteristic length scale is on the order of microns.

Recently, several researchers have suggested that the no-slip boundary condition may not be suitable at both the micro- and nano-scale. Ruckenstein and Rajora [2] investigated fluid slip in glass capillaries with surfaces made repellent to the flowing liquid. Their experimental results of pressure drop indicate larger slip than that predicted by chemical potential theory, where slip is proportional to the gradient in the chemical potential. The results suggest that slip occurs over a gap near the surface rather than directly on the solid surface, and the gap forms when a hydrophobic liquid flows over a hydrophilic surface and vice versa. They suggest the gap may be increased in thickness by the release of gases entrained in the flowing liquid and/or the desorption of soluble gases. Their results, however, are inferred from pressure drop-flow measurements and not direct measurement of the fluid velocities. Computationally, Barrat and Bocquet [3] expect significant slip in nanoporous medium when the liquid is sufficiently non-wetting, which increases the effective permeability of the nanoporous medium. Their predictions are experimentally justified by Churaev et. al. [4] who postulated slip at the wall to recover the viscosity of water for water flow in thin (<1μm) hydrophobic capillaries. Pit et. al. [5] observe fluid slip for hexadecane between two rotating parallel disks with a gap of 190 microns. By following the movement of a photo-bleached test section, they measure no slip when the surfaces are coated with perfluorodecanetrichlorosilane, a slip length of approximately 170nm for bare sapphire, and a slip length of 400nm for an octadecyltrichlorosilane (OTS) coating. They conclude that slip depends on both the interfacial energy and surface roughness. At a much smaller length scale, Craig et. al. [6] calculate the drainage force for a sphere approaching a solid, flat wall. They measure slip lengths up to 20nm for aqueous sucrose solutions that have advancing and receding contact angles of 70 and 40 degrees respectively. They conclude that the slip length depends non-linearly on the approach rate of the sphere. Zhu and Granick [7] experimentally observe fluid slip in an oscillating surface force apparatus. For cylinder separations from approximately 10-200nm, they measure slip lengths of up to 2.5μm for water between octadecyltriethoxysilane (OTE) surfaces, 1.5μm for tetradecane between OTE surfaces, and 0.9μm for tetradecane between mica surfaces. Their results suggest a strong dependence between the velocity gradient and magnitude of the slip, a critical shear rate for onset of fluid slip, and an increase in the slip length as the separation between the cylinders decreases. Their conclusions, however, are inferred from discrepancies between the measured normal force and expected normal force assuming no-slip, and are not measured directly. More recently, Zhu and Granick [8] examine the relative importance of surface roughness and fluid-surface interactions in determining the appropriate boundary condition. For similar, poorly wetting surfaces the critical shear rate to observe deviations from force predictions assuming no-slip increased nearly exponentially with increasing surface roughness. They conclude that local intermolecular interactions are dominate when surfaces are very smooth, but are otherwise negligible at sufficient surface roughness. Tretheway and Meinhart [9] measured fluid velocities in hydrophilic and hydrophobic microchannels by micron resolution particle image velocimetry (μ-PIV). Their results showed a significant fluid velocity near a hydrophobic microchannel wall and no-slip for a hydrophilic surface. A slip length of 0.92 microns was estimated.

In this work, we examine the slip boundary condition, address the validity of Navier's hypothesis with Lattice Boltzmann simulations, and compare the simulations to the results of Tretheway and Meinhart [9].

EXPERIMENTS

In this section, we review the results for fluid flow through hydrophilic and hydrophobic microchannels. Details of the techniques and experimental apparatus can be found in Tretheway and Meinhart [9].

Velocities were measured by micron-resolution particle image velocimetry (μ-PIV) in 30μm deep by 300μm wide extruded glass microchannels trimmed to a length of 8.25cm. Measurements were made 4 to 4.5cm from the edge to eliminate possible entrance effects and to ensure a fully developed flow profile. Deionized water seeded with 300nm fluorescent particles was injected into the channel at a constant flow rate of 200μl/hr. Two channel types were examined, hydrophilic and hydrophobic. An untreated glass channel is naturally hydrophilic. Hydrophobic microchannels are created by coating the walls with octadecyltrichlorosilane (OTS). The smooth and robust monolayer is approximately 2.3nm thick with a roughness of 2-3 angstroms. The OTS layer thickness is less than $1/10000^{th}$ the depth of the microchannel. Two images separated by 150μs were captured on a cooled, interline CCD camera and analyzed with PIV software developed by Steve Wereley (currently at the Dept. of Mechanical Eng., Purdue University). The interrogation region is 128 x 8 pixels (streamwise to spanwise), which yields a spatial resolution of 14.7x0.9x1.8μm with velocity measurements obtained to within 450nm of the wall. The out of plane measurement depth is approximately 1.8μm. To increase signal-to-noise, 49 image pairs are cross correlated. The resulting correlation functions are then averaged before peak detection, following the algorithm given by Meinhart et. al. [10].

Figure 1 shows the average velocity profile for flow near the wall for hydrophilic (squares) and hydrophobic (triangles) microchannel surfaces. The velocity profiles are normalized by

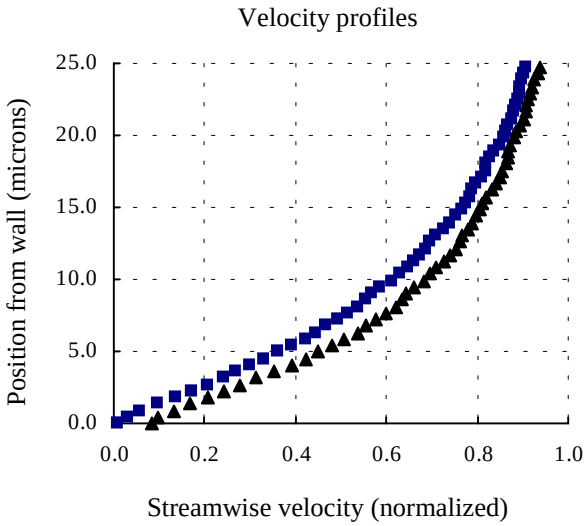

Figure 1. Experimental velocity profiles for flow over a hydrophilic (blue squares) and hydrophobic (black triangles) microchannel surface. The velocity profiles are normalized with the free-stream velocity.

the free-stream velocity. Measurements are taken in the mid-plane of the channel (15μm from the bottom) near the side wall. The field of view is aligned such that a section of the wall is included in each image. Since there are no particles in the wall, the resulting correlations for that region produce erroneous velocity vectors with magnitudes and directions that are inconsistent with the known direction of flow. The wall location is then set at the point at which the velocity vectors are erroneous. The uncertainty of the wall location is approximately 450nm.

For a hydrophilic surface (squares), Figure 1 shows the velocity approaching its free-stream value at 25μm from the wall and smoothly decreasing to zero at the wall. This profile is consistent with the analytical solution for flow through a rectangular duct with a finite aspect ratio, assuming the no-slip boundary condition. For flow through a hydrophobic microchannel, the velocity profile is significantly different. While Figure 1 shows the hydrophobic velocity profile (triangles) near its free-stream value at 25μm and decreasing towards the wall, a finite and significant velocity is measured within 450nm above the wall. This slip velocity is approximately 8.5% of the free-stream velocity, and effectively shifts the entire velocity profile when compared with the no-slip profile (squares). As a result, the velocity 25μm from the wall in a hydrophobic microchannel is approximately 95% of the free-stream velocity, compared with 90% for a microchannel that is hydrophilic. Thus, a monolayer of hydrophobic molecules with a thickness of less than 23 angstroms significantly affects the velocity profile even out to a distance of 25 microns from the wall.

The results of Figure 1 provide a direct measurement of fluid slip for water flowing over a hydrophobic surface, and confirm the no-slip boundary condition for water flowing over a hydrophilic surface. From these measurements we calculate a slip length, β, of approximately 0.92μm. This is consistent with the work by Zhu and Granick [7] and Pit et. al. [5] who report slip lengths up to 2μm. Since the current experiments are limited to a narrow range of flow rates, we are unable to determine if the slip velocity is proportional to the shear stress, with β being a constant.

LATTICE BOLTZMANN SIMULATIONS

Methodology

The Lattice Boltzmann Method (LBM) is an alternative to the traditional numerical methods for solving incompressible Navier-Stokes equations. Instead of solving for the velocity and pressure directly, LBM involves the particle distribution functions $f(\mathbf{x},\boldsymbol{\xi},t)$ (where $\mathbf{x}$ is the space coordinate and $\boldsymbol{\xi}$ is the particle velocity) based on a simplified Boltzmann equation (the LBGK model [11,12]), which can be written as follows

$$\frac{\partial f}{\partial t}+\xi\cdot\frac{\partial f}{\partial x}=-\frac{1}{\tau}\left(f-f^{0}\right) \tag{3}$$

where τ is the relaxation time and f^0 is the equilibrium distribution function. The term, $-(f-f^0)/\tau$ is the well known BGK approximation [13] to the complex collision operator in the Boltzmann equation. The particle velocity space, $\boldsymbol{\xi}$, can be discretized by a finite set of velocities, $\{\boldsymbol{\xi}_j, j=0,1,2,\ldots n\}$. With $f_j(x,t)$ the distribution function for $\boldsymbol{\xi}_j$, we have

$$\frac{\partial f_j}{\partial t}+\xi_j\cdot\frac{\partial f_j}{\partial x}=-\frac{1}{\tau}\left(f_j-f_j{}^{0}\right) \tag{4}$$

After discretization in time, the lattice Boltzmann equation (LBE) is obtained

$$f_j(x+\xi_j\Delta t,t+\Delta t)=f_j(x,t)-\frac{1}{\tau}(f_j-f_j^0) \tag{5}$$

where the term $-(f_j-f_j^0)/\tau$ represents the collision (note that the collision is implicitly defined in LBM). Beginning with the initial distribution and the distribution at time t=0, which can be taken as the initial equilibrium distribution, the entire one-step computation (from time t to $t+\Delta t$) can be divided into two steps: first, compute the collision and update the distribution at time t by summing the collision terms; and second, compute the distribution at time $t+\Delta t$ by streaming the post-collision distribution function, i.e. the computed right hand side of the LBE. With the new distribution function obtained, the macroscopic quantities of density, $\rho(\mathbf{x},t)$, and momentum $\rho\mathbf{u}(\mathbf{x},t)$ can be calculated simply at all lattice points by

$$\rho(x,t)=\sum_j f_j(x,t) \tag{6}$$

$$\rho u(x,t)=\sum_j \xi_j f_j(x,t) \tag{7}$$

We use a standard three-dimensional lattice D3Q19 which has 19 discrete particle velocities and can be written as follows:

$$\xi_j=\begin{cases}(0,0,0) & j=0\\ (\pm1,0,0),(0,\pm1,0),(0,0,\pm1) & j=1,2,\ldots6\\ (\pm1,\pm1,0),(\pm1,0,\pm1),(0,\pm1,\pm1) & j=7,8,\ldots18\end{cases} \tag{8}$$

For athermal fluids, the equilibrium distribution function $f_j^0(\rho,\mathbf{u})$ in the D3Q19 lattice can be computed by

$$f_j^0(\rho,u) = \rho\, w_j(1+3\xi_j\cdot u+\frac{9}{2}(\xi_j\cdot u)^2-\frac{3}{2}u\cdot u) \qquad (9)$$

where the w_j is the weight, which takes the values:

$$w_j = \begin{cases} 1/3 & j=0 \\ 1/18 & j=1,2,...6 \\ 1/36 & j=7,8,...18 \end{cases} \qquad (10)$$

The LBM used in our simulation is standard. Readers interested in these methods can see Rothman and Zaleski [14], Chen and Doolan [15}, Luo [16], He and Luo [17], or Hou [18] and the references therein. Due to the large amount of literature on LBM, the references here are far from complete.

Our simulations focus on the modeling of the no-slip and partial slip boundary conditions. In LBM, the bounce-back scheme is widely used to treat the no-slip boundary condition (with the exception Nie et. al [19], who studied velocity slip in MEMS flows), while specular reflection can be used to model the slip boundary condition. In this work, we apply the standard bounce-back scheme to simulate a no-slip boundary and a combination of standard bounce-back and specular reflection to model the partial slip boundary by assigning the probability, *P*, of bounce-back and the probability, 1-*P*, of specular reflection when a distribution hits a wall. To the best of our knowledge this is the first time this combination has been applied in the lattice Boltzmann context. However, the idea was mentioned by Luo [20] and can be dated back to 1867 when Maxwell [21] studied the microscopic modeling of the solid boundary. It has been used previously by Lavallee et. al. [22] to treat the no-slip boundary condition in the lattice gas method, and has been used in the context of Direct Simulation Monte Carlo [23]. The combination of bounce-back and specular reflection is hard to implement in complex geometries. For a newly developed method to treat slip and partial-slip boundary conditions for arbitrary complex boundaries in lattice Boltzmann simulations, see Zhou [24].

In the LBM simulations we closely match the parameters in the experiment, with the exception of the channel length. In the experiments the length is 8.25cm, while the simulations set the length to twice the channel width (600mm) and employ a periodic boundary condition along the channel direction at the entrance and end of the channel. The simulations are done on a 20x200x400 grid with computations continued until the flow reaches a steady state.

Results

Figure 2 shows the velocity profile of the exact solution of the Navier-Stokes equations assuming no-slip at the walls (intermittent, black line), the velocity profile measured experimentally with μ-PIV (blue squares), and the LBM simulations assuming 100% bounce-back at the wall elements (solid, red line). The LBM simulations are quantitatively consistent with both the analytical solution and the experimental results. Thus, a probability of bounce-back equal to 1 produces the no-slip boundary condition. The excellent quantitative agreement confirms the validity of the LBM technique as well as validates the experimentally measured velocity profile.

With the LBM technique validated, we examine the probability required to generate slip lengths in the range of

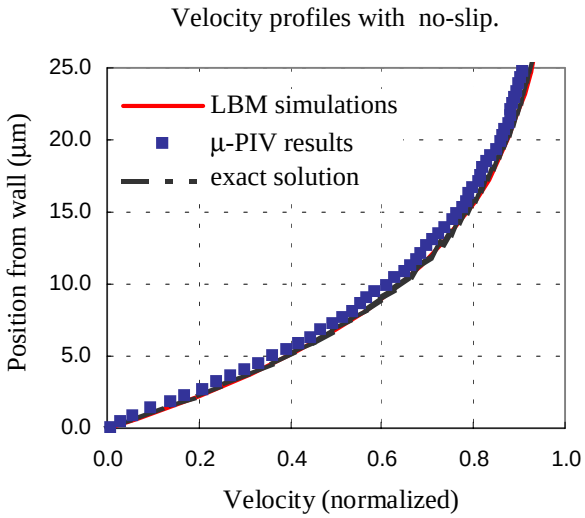

Figure 2. Velocity profiles for a hydrophilic surface measured with μ-PIV (blue squares), LBM simulations assuming a probability of bounce-back of 1.0 (solid, red line), and the exact solution (intermittent, black line)

experimentally measured values. Figure 3 shows the slip length, β, as a function of the probability of bounce-back. As expected, the slip length increases as the probability of bounce-back decreases (and thus the specular reflection increases). Tretheway and Meinhart [9] calculate a slip length equal to 0.92μm. From Fig. 3, this would correspond to a very low bounce-back probability, between 0.03 and 0.04 (or a specular reflection probability between 0.96 and 0.97).

Figure 4 compares the velocity profile measured by μ-PIV for flow over a hydrophobic surface [9] to the numerically calculated LBM profile assuming a probability of bounce-back equal to 0.03. The assumed probability, *P*=0.03, produces a similar slip length and slip velocity at the wall. The profiles show good agreement. Thus, the LBM simulations may be used to explore the slip condition.

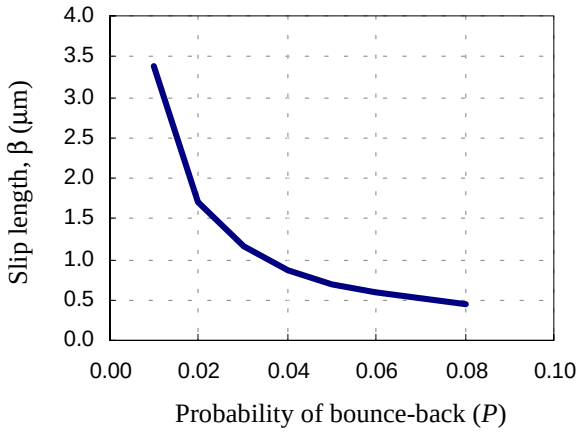

Figure 3. Slip length (β) as a function of the probability of bounce back in LBM simulations in a 30x300μm channel..

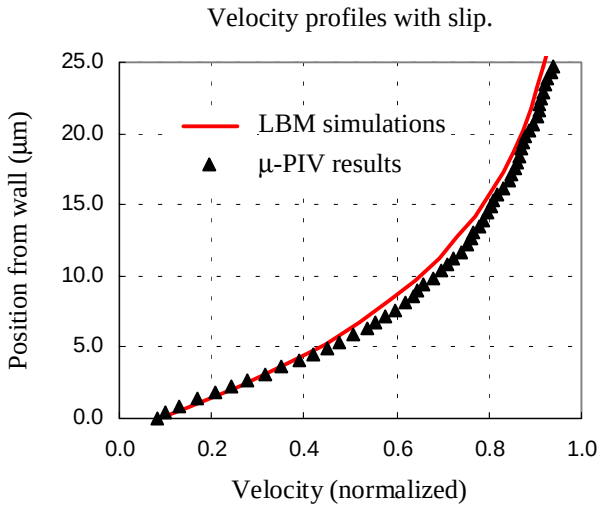

Figure 4. Velocity profiles for a hydrophobic surface measured with μ-PIV (black triangles) and LBM simulations assuming a probability of bounce-back of 0.03 (solid, red line).

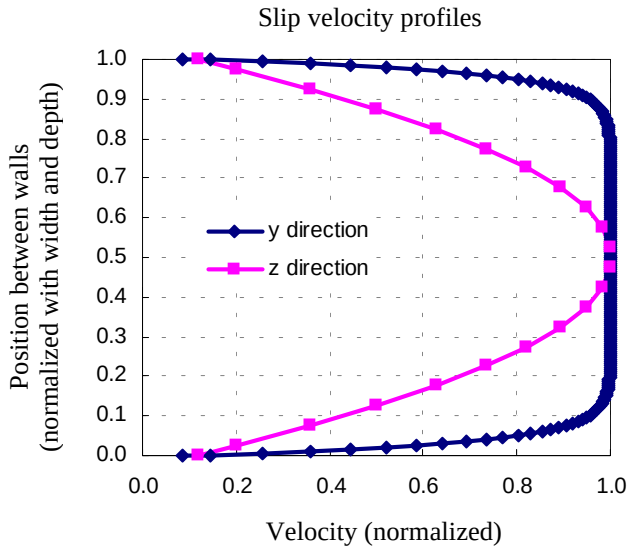

Figure 5. Normalized velocity profiles in the y (width 300μm) and the z (depth 30μm) directions.

DISCUSSION

For the lattice Boltzmann simulations we use a 20x200x400 (z,y,x) mesh in calculating the velocity profiles. If we compare this results with coarser meshes we observe that the calculated slip length and resulting slip velocity depend on the mesh spacing with the calculated slip length and slip velocity for a given probability of bounce-back decreasing with mesh refinement. For the 20x200x400 mesh, the slip length and slip velocity for P=0.03 were calculated to be 1.15μm and 8.74% respectively. This compares to a calculated slip length and slip velocity of 1.72μm and 27.93% for a 5x50x100 mesh and 1.33μm and 16.02% for a 10x100x200 mesh. The results presented in this paper with a 20x200x400 mesh is at our current computational limit. Future work with mesh refinement will continue until the slip length and slip velocity no longer varies with mesh size.

Tretheway and Meinhart [9] measured velocity profiles at the mid-plane of the side-wall of the channel (in the y direction, width of 300μm). While we are currently unable to experimentally measure the velocity in the z (or depth, 30μm) direction, the LBM simulations show, for a given probability of bounce-back, that the slip velocity varies along the channel wall. Figure 5 shows the velocity profiles at the mid-plane for both the z and y directions. While the calculated slip lengths are nearly identical for both the z and y walls (1.12 for the z direction and 1.15 for the y direction), the calculated slip velocities are substantially different, 8.74% of the free stream velocity for the y direction and 11.95% for the z direction. Even though the slip length is smaller for the z direction, the slip velocity is larger. This difference results from variations in the shear rate along the walls of the channel and produces a more complex velocity than expected from previous results for flow between two infinite parallel plates. For the previous case, the velocity profile that develops as a result of slip at the surface is a simple combination of the velocity profile assuming no-slip and a given slip velocity. This simple combination is not necessarily valid for channel flow or arbitrarily enclosed geometries.

Navier's hypothesis proposes that the velocity is proportional to the shear rate at the wall with the slip length, β, a constant. Pit et. al. [5] estimate a slip length equal to 0.4μm and conclude that it remains constant up to a shear rate of $2000s^{-1}$. Zhu and Granick [7] and Craig et. al [6] conclude that the slip length varies with shear rate with Zhu and Granick [7] identifying a critical shear rate for slip to develop. The experimental range of shear rates examined by Tretheway and Meinhart [9] are too narrow to conclude the slip length dependence on shear rate. We've examined by LBM the slip length as a function of shear rate for flow between two infinite parallel plates. The simulations indicate that for a given probability of bounce-back, the slip length remains constant from a shear near $20s^{-1}$ to nearly $2000s^{-1}$. This agrees with the results of Pit et. al [5], however the results are for flow between two infinite parallel plates. Currently, we are examining by LBM variations in shear rate for flow through a channel.

CONCLUSIONS

In this work we examine the slip boundary condition by lattice Boltzmann simulations and compare the results to the μ-PIV results of Tretheway and Meinhart [9]. The simulations are consistent with the measured velocity profiles for the hydrophilic (no-slip) channels when the probability of bounce-back is equal to 1 and for the hydrophobic (slip) channels when the probability of bounce-back equals 0.03 to 0.04. In addition, the no-slip results are consistent with the analytical solution of the Navier Stokes equations assuming no-slip. The simulations indicate that, while the slip length remains nearly constant (slightly lower in the depth direction), the slip velocity varies with the wall position in the channel as a results of variations in shear rate with higher slip velocities in the depth direction.

Thus, the resulting velocity profile in a channel flow is more complex than a simple combination of the no-slip solution and slip velocity as is the case for flow between two infinite parallel plates.

ACKNOWLEDGMENTS

This work is supported by Grant Nos. NSF CTS-9874839, NSF ACI-0086061, and DARPA/Air Force 30602-00-2-0609.

REFERENCES

[1]Navier, C. L. M. H. (1823) Memoirs de l'Academie Royale des Sciences de l'Institut de France, 1, 414-416.

[2]Ruckenstein, E. and Rajora, P. (1983) "On the No-Slip Boundary Condition of Hydrodynamics". J. of Colloid and Interface Science, **96**, 488-491.

[3]Barrat, J. and Bocquet, L. (1999) "Large Slip Effect at a Nonwetting Fluid-Solid Interface". Physical Review Letters, **82**, 4671-4674.

[4]Churaev, N., Sobolev, V., and Somov, A. (1984) "Slippage of Liquids Over Lyophobic Solid Surfaces". J. of Colloid and Interface Science, **97**, 574-581.

[5]Pit, R., Hervet, H., and Leger, L. (2000) "Direct Experimental Evidence of Slip in Hexadecane: Solid Interfaces". Physical Review Letters, **85**, 980-983.

[6]Craig, V., Neto, C., and Williams, D. (2001) "Shear-Dependent Boundary Slip in an Aqueous Newtonian Liquid". Phys. Rev. Lett. **87**, 054504.

[7]Zhu Y., and Granick S. (2001) "Rate-Dependent Slip of Newtonian Liquids at Smooth Surfaces". Phys. Rev. Lett. **87**, 096105.

[8]Zhu, Y., and Granick, S. (2002) "Limits of Hydrodynamic No-Slip Boundary Condition". Phys. Rev. Lett. **88**, 106102.

[9]Tretheway, D. and Meinhart, C. (2002) "Apparent Fluid Slip at Hydrophobic Microchannel Walls". Physics of Fluids **14**, L9-L12.

[10]Meinhart, C., Wereley, S., and Santiago, J. (2000) "A PIV Algorithm for Estimating Time-Averaged Velocity Fields". J. Fluids Eng. **122**, 285.

[11]Qian, Y.H. (1990) "Lattice Gas and Lattice Kinetic Theory Applied to the Navier-Stokes Equations". Ph.D. Thesis, University Pierre et Marie Curie, Paris.

[12]Chen, S.Y., Chen, H.D., Martinez, D., and Matthaeus, W. (1991) "Lattice Boltzmann Model for Simulation of Magnetohydrodynamics". Phys. Rev Lett. **67**, 3776-3779.

[13]Bhatnager, P.L., Gross, E.P., and Krook, M. (1954) "A Model for Collision Processes in Gases, I: Small Amplitude Process in Charged and Neutral One-Component System". Phys. Rev. **94**, 511-525.

[14]Rothman, D.H. and Zaleski S. (1994) "Lattice Gas Models of Phase Separation: Interface, Phase Transitions, and Multiphase Flow". Rev. Mod. Phys. **66**, 1417-1479.

[15]Chen, S.Y. and Doolen, G.D. (1998) "Lattice Boltzmann Method for Fluid Flows". Ann. Rev. Fluid Mech. **30**, 329-364.

[16]Luo, L-S. (1998) "Unified Theory of the Lattice Boltzmann Models for Nonideal Gases". Phys. Rev Lett. **81**, 1618-1621.

[17]He, X. and Luo, L-S. (1997) "Theory of Lattice Boltzmann Method: From the Boltzmann Equation to the Lattice Boltzmann Equation". Phys. Rev. E **56**, 6811-6817.

[18]Hou, S. (1995) "Lattice Boltzmann Method for Incompressible Viscous Flow". Ph.D. Thesis, Kansas State University.

[19]Nie, X., Doolen, G.D., and Chen, S.Y. (2002) "Lattice Boltzmann Simulations of Fluid Flows in MEMS". J. Stat. Phys. **107**, 279-289.

[20]Luo, L-S. (1998) "Future of Lattice-Gas and Lattice Boltzmann Methods". Proc. of a Workshop on Computational Aerosciences in the 21st Century, pp. 165-187, (Kluwer, Dordrecht, 2000).

[21]Maxwell, J.C. (1867) Phil. Trans. R. Soc. London, Ser. A **170**, 231.

[22]Lavallee, P., Boon, J.P., and Noullez, A. (1991) "Boundaries in Lattice Gas Flows". Physica D **47**, 233-240.

[23]Bird, G.A. (1994) "Molecular Gas Dynamics and the Direct Simulation of Gas Flows". Oxford Science Publications.

[24]Zhou, J.G. (2001) "An Elastic-Collision Scheme for Lattice Boltzmann Methods". Int. J. Mod. Phys. C **12**, 387.

